RSC Advances

PAPER

View Article Online
View Journal | View Issue

Cite this: *RSC Adv.*, 2017, **7**, 50663

Reactive molecular dynamics study of the decomposition mechanism of the environmentally friendly insulating medium C_3F_7CN†

Xiaoxing Zhang,[a] Yi Li,[a] Dachang Chen,[a] Song Xiao,*[a] Shuangshuang Tian,[a] Ju Tang[a] and Ran Zhuo[b]

The extensive use of sulfur hexafluoride (SF_6) gas in the power industry has a strong greenhouse effect. Hence, many scholars are committed to studying SF_6 alternative gases to achieve green power development. In the past two years, C_3F_7CN (heptafluoroisobutyronitrile) has attracted the attention of many scholars due to its excellent insulation and environmental protection characteristics as a potential alternative gas. This study theoretically explores the decomposition characteristics of C_3F_7CN and the C_3F_7CN/CO_2 gas mixture based on the reactive molecular dynamics method and density functional theory. The main decomposition pathways of C_3F_7CN and the enthalpy of each path at different temperatures were analyzed. The yield of the main decomposition products was obtained under several temperature conditions. The decomposition of C_3F_7CN mainly produced CF_3, C_3F_7, CN, CNF, CF_2, CF, F, and other free radicals and a few molecular products, such as CF_4 and C_3F_8. The C_3F_7CN/CO_2 gas mixture has more excellent decomposition characteristics than that of the pure C_3F_7CN. The addition of CO_2 effectively ensures that the gas mixture has a low liquefaction temperature, which is considerably suitable for use as a gas insulation medium. The relevant research results provide guidance for the further exploration on the electrical properties and practical engineering application of the C_3F_7CN gas mixture.

Received 7th September 2017
Accepted 18th October 2017

DOI: 10.1039/c7ra09959b

rsc.li/rsc-advances

1 Introduction

SF_6 (sulfur hexafluoride) is the most common insulation medium used in high-voltage (HV) electrical equipment such as gas insulated switchgear (GIS).[1] However, SF_6 is a greenhouse gas (GHG) regulated under the Kyoto Protocol with a global warming potential (GWP) of 22 800.[2,3] Although the proportion of greenhouse effect caused by the use of SF_6 is not as large as the amount of fossil fuel energy consumed, the global atmospheric content of SF_6 has increased by 20% in the past five years and the atmospheric mole fraction of SF_6 is 7.28 ppq currently corresponding to a radiative forcing of 0.0041 w m^{-2}.[4,5] THe greenhouse effect has caused widespread public concern in recent years.[6] Climate deterioration caused by SF_6 has gradually become one of the contradictions between power industry development and environmental protection. Hence, the power industry should gradually limit the use of SF_6 and search for an environmentally friendly alternative gas for SF_6 in gas-insulated equipment.

C_3F_7CN (heptafluoroisobutyronitrile) is a potential alternative gas for SF_6 (see Fig. 1 for its molecular structure) with a GWP value of 2100 and Ozone Depression Potential (ODP) value of 0.[4] The dielectric strength of C_3F_7CN is 2.74 times that of SF_6.[7] It should be used in combination with CO_2 or other buffer gases with low liquefaction temperature due to its high liquefaction temperature (*i.e.*, −4.7 °C). In addition, the toxicity of the C_3F_7CN/CO_2 gas mixture with C_3F_7CN volume fraction below 10% is lower than that of pure SF_6. Thus, the former is harmless to humans.[8] These physical and chemical properties indicate that C_3F_7CN is excellent in terms of environmental protection, insulation and safety, and has immense potential to replace SF_6.

In the past two years, many scholars have proven that the C_3F_7CN/CO_2 gas mixture has excellent insulation and arc extinguishing performance through numerous tests.[3,7–10] For engineering applications, a gas insulated line (GIL) with a rated voltage of 420 kV and a current transformer (CT) with a rated voltage of 245 kV using the C_3F_7CN/CO_2 gas mixture as insulating medium were tested in 2015.[3,8] In addition, the investigation of the decomposition properties of a gas-insulating medium is an important component to comprehensively evaluate its performance. On the one hand, the insulation defects

[a]*School of Electrical Engineering, Wuhan University, BaYi Street No. 299, Wuhan 430072, Hubei Province, China. E-mail: xiaosongxs@gmail.com; Tel: +86 18986238962*

[b]*Electric Power Research Institute, China Southern Power Grid, Guangzhou 510623, China*

† Electronic supplementary information (ESI) available. See DOI: 10.1039/c7ra09959b

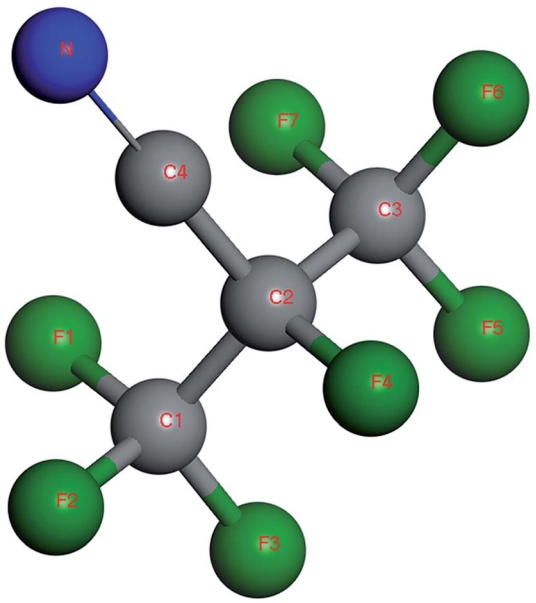

Fig. 1 Molecule structure of C_3F_7CN.

caused by aging under long-term operating conditions in electrical equipment will lead to partial discharge (PD) or flashover and is accompanied by the decomposition of the insulating medium. The local overheating fault can also lead to the decomposition of the insulating medium. On the other hand, the decomposition characteristics of the insulating medium are closely related to its self-recovery characteristics and arc-extinguishing properties.

At present, researches on the decomposition characteristics of C_3F_7CN have achieved noteworthy results. Kieffel *et al.* investigated the pyrolysis characteristics of the C_3F_7CN/CO_2 gas mixture. They found the initial decomposition temperature of C_3F_7CN was 650 °C, thereby mainly producing decomposition products, such as CO, CF_3CN, and C_2F_5CN.[8] Andersen *et al.* investigated the atmospheric chemistry of C_3F_7CN and evaluated its environmental effects based on density functional theory and infrared spectroscopy.[11] Our team has explored the decomposition mechanism of C_3F_7CN in the presence of trace water impurity through quantum chemical calculation. The ionization parameters of C_3F_7CN and various decomposition products were analyzed from the perspective of molecular structure, thereby providing a theoretical reference for the further study of the C_3F_7CN decomposition characteristics.[12]

At present, only a few studies have been conducted on the decomposition characteristics of the C_3F_7CN/CO_2 gas mixture. Our previous studies on the decomposition mechanism of C_3F_7CN were from the perspective of individual molecule and did not consider the decomposition process in multi-molecular and gas mixture systems. In this paper, we constructed the multi-molecular and C_3F_7CN/CO_2 gas mixture model to study the decomposition process of C_3F_7CN using the reactive force field molecular dynamics (ReaxFF-MD) method and density functional theory (DFT). The decomposition paths, reaction enthalpy, and products distribution of the C_3F_7CN gas mixture at different temperatures were firstly investigated. Relevant results provide guidance for further exploration on electrical properties and practical engineering application of C_3F_7CN gas mixture.

2 Theoretical methods and computational details

2.1 ReaxFF-MD simulation details

ReaxFF is based on bond order to describe the dissociation and formation of covalent bonds at the atomic level[13] and is a beneficial tool for studying chemical reactions and predicting the performance of new materials. During the past more than ten years, ReaxFF has been used to treat a variety of elements

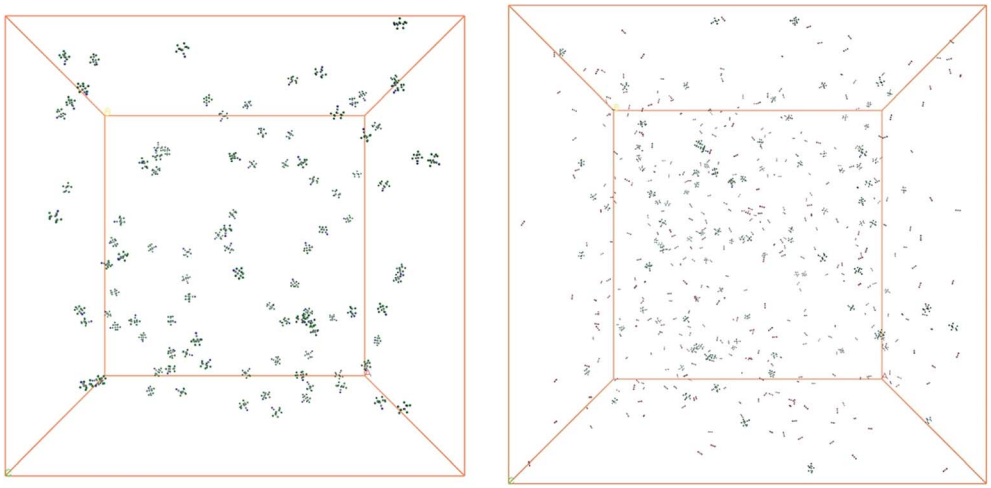

a) C_3F_7CN system b) C_3F_7CN/CO_2 system

Fig. 2 Configurations of the C_3F_7CN and C_3F_7CN/CO_2 systems.

and multifunctional systems and is suitable for describing polyatomic systems.[14–16] The energy expression of ReaxFF is presented as follows:

$$E_{system} = E_{bond} + E_{over} + E_{under} + E_{val} + E_{pen} + E_{tors} + E_{conj} + E_{vdWaals} + E_{Coulomb,} \quad (1)$$

where E_{bond} corresponds to bond energy; E_{over} and E_{under} denote the over and under coordinated atoms, respectively, in the energy contribution; E_{val}, E_{pen}, E_{tors}, E_{conj}, $E_{vdWaals}$, and $E_{Coulomb}$ represent the valence angle term, penalty energy, torsion energy, conjugation effects to energy, nonbonded van der Waals interaction, and Coulomb interaction, respectively.

Two periodic cubic boxes were built to explore the decomposition of C_3F_7CN and the C_3F_7CN/CO_2 gas mixture (see Fig. 2). The C_3F_7CN system contains 100 C_3F_7CN molecules with a density of 0.00811 g cm^{-3}. The length of the box is 159 Å. At present, many scholars have tested the insulation characteristics of C_3F_7CN/CO_2 mixture and found that mixtures with 20% C_3F_7CN displayed dielectric strengths comparable to SF_6.[4,7] In order to reveal the decomposition properties of mixtures in this scale, we built the C_3F_7CN/CO_2 system which contains 100 C_3F_7CN molecules and 400 CO_2 molecules with a density of 0.00351 g cm^{-3}. The length of the box is 260 Å. The initial density corresponds to the actual density of C_3F_7CN under 25 °C and 0.1 Mpa. The system was minimized with the NVE ensemble for 5 ps at 5 K and equilibrated with the NVT ensemble thereafter for 10 ps at 1000 K using a time step of 0.1 fs.[16] The NVT simulations were then conducted at different temperatures for 1000 ps to explore the decomposition process of C_3F_7CN and C_3F_7CN/CO_2 gas mixture. The temperature was controlled by the method of a Berendsen thermostat with a 0.1 ps damping constant.[17] All the ReaxFF-MD simulations in this paper were performed based on the ReaxFF module of ADF (Amsterdam Density Functional).[18]

2.2 DFT calculation details

The first principle of calculations based on the density functional theory (DFT) was performed to obtain the precise dissociation energy of C_3F_7CN at different temperatures. This theory is widely used in the study of chemical reaction mechanisms, and can describe any given chemical system with high accuracy.[19–21]

The spin unrestricted DFT calculation in the current study was performed based on the Dmol 3 module of the Materials studio 8.0. The meta-generalized approximation (mGGA) method treated by M06L functions is used to describe the exchange-correlation energy. This local density functional does well for predicting geometries and vibrational frequencies and gives great performance for a combination of main-group thermochemistry and thermochemical kinetics.[22,23] The double numerical atomic orbital augmented by d-polarization (DNP) is used as the basis set. Geometry optimizations were performed with the following convergence parameters: (1) energy convergence tolerance of 1.0×10^{-5} Ha, (2) maximum force of 0.002 Ha $Å^{-1}$, and (3) maximum displacement of 0.005 Å. It should be pointed that spin contamination (unrestricted DFT is much less affected by it than unrestricted Hartree–Fock theory[24]) and wave function unstability may occur in spin unrestricted calculation. The self-consistent-field (SCF) solution stability is checked to ensure the accuracy of calculation results.

The enthalpy correction is presented as follows to obtain the precise energy of the system at a given temperature:[25]

$$\Delta E = \sum(E_{product} + \Delta E_{product}) - \sum(E_{reactant} + \Delta E_{reactant}), \quad (2)$$

where $E_{product}$ and $E_{reactant}$ correspond to the energy of the product and reactant, respectively, at 0 K and $\Delta E_{product}$ and $\Delta E_{reactant}$ correspond to the correcting values of the enthalpy of product and reactant, respectively, at a given temperature.

3 Results and discussion

3.1 Decomposition of the pure C_3F_7CN

3.1.1 Decomposition process and main reaction paths. The three main types of discharges in electrical equipment are the corona (partial discharge), arc, and spark discharges, wherein the corona and arc discharges are the most common.[26] The maximum temperature in the central region of the corona discharge is in the range of 700–1200 K and the highest temperature in the arc discharge region can reach 12 000 K.[26–28] The current study analyzed the decomposition mechanism of C_3F_7CN and its gas mixture at different temperatures to clarify the particle composition and product change. It should be noted that the time scale of ReaxFF MD simulation is normally limited to several dozens of nanoseconds due to the computational cost.[28,29] Hence, we enhance the temperatures to accelerate the simulation process to allow reactions can be observed.

First, the multi-molecular ReaxFF molecular dynamic simulations of C_3F_7CN were performed and demonstrated that the C_3F_7CN molecule began to decompose at 1900 K. Fig. 3 shows the time evolution of the major species of the C_3F_7CN decomposition at 1900 K. Table 1 shows the generation time of the major species and corresponding decomposition pathways. At 1900 K, the C_3F_7CN decomposition mainly produces free radicals, such as CF_3, C_3F_7, CN, CNF, CF_2, CF, $CF_3CFCN(C_3NF_4)$, and F. It is important to note that some free radicals, such as

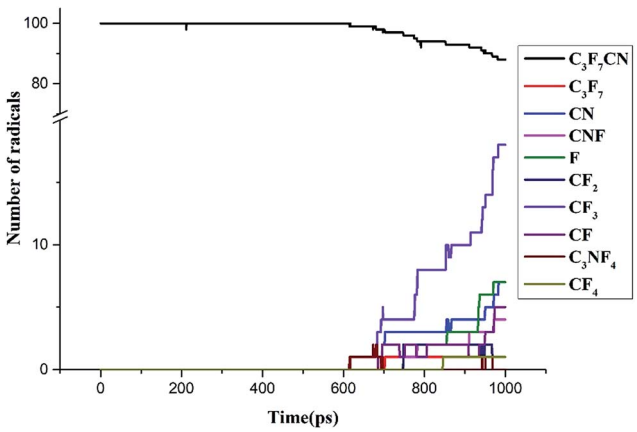

Fig. 3 Time evolution of the major species at 1900 K.

Table 1 Generation time of the major species and corresponding decomposition pathways

Major species	Generation time (ps)	Reaction		ΔE^a (kcal mol^{-1})
C_3NF_4, CF_3	615	A	$C_3F_7CN \rightarrow CF_3 + CF_3CFCN$	72.67
C_3F_7	702.5	B	$C_3F_7CN \rightarrow C_3F_7 + CN$	101.33
C_4F_6N	—	C	$C_3F_7CN \rightarrow (CF_3)_2CCN + F$	89.17
CN, CF	685.625	D	$CF_3CFCN \rightarrow CF_3 + CF + CN$	174.66
CF_2, F	748.125	E	$CF_3 \rightarrow CF_2 + F$	79.04
CNF	748.125	F	$CN + F \rightarrow CNF$	−118.48
CF_4	845.625	G	$CF_3 + F \rightarrow CF_4$	−107.64
C	—	H	$CF \rightarrow C + F$	121.23

[a] $T = 1900$ K, at mGGA-M06L level with ZPE and enthalpy corrections.

CN, are harmful free radicals and could produce toxic molecules. The content and toxicity of the decomposition products of C_3F_7CN need further test study before engineering application.

C_3F_7CN began to decompose at 615 ps, thereby producing CF_3CFCN and CF_3. This reaction path is required to absorb 72.67 kcal mol^{-1}. Another decomposing path began at 702.5 ps, thereby producing C_3F_7 and CN and needs to absorb 101.33 kcal mol^{-1}. In addition, the decomposition of CF_3CFCN is at 685.625 ps, thereby generating CF_3, CF, and CN. CF_3 can further decompose to CF_2 and F by absorbing 79.04 kcal mol^{-1}, CF can further decompose to C and F by absorbing 121.23 kcal mol^{-1}. CF_4 is one of the stable decomposition products, which is formed by CF_3 and F and releases −107.64 kcal mol^{-1}. In addition, the DFT calculation results show that the energy required for path A is lower than that for path B, which means that path A is more likely to occur than path B. And the ReaxFF-MD results show that the number of generated CF_3 increases rapidly during 700–1000 ps, which indicates the results of ReaxFF are consistent with DFT calculations and the performance of ReaxFF is reliable.

3.1.2 Effect of temperature on the decomposition process. To further analyze the influence of temperature on the decomposition process of C_3F_7CN, the molecular dynamic simulation of the C_3F_7CN system was performed at five temperature zones, that is, 1900 K, 2000 K, 2100 K, 2200 K, and 2400 K, for a total simulation time of 1000 ps.

Fig. 4 shows the time evolution of the potential energy between 1900 K and 2400 K. The potential energy of the system increases during the reaction process at different temperatures,

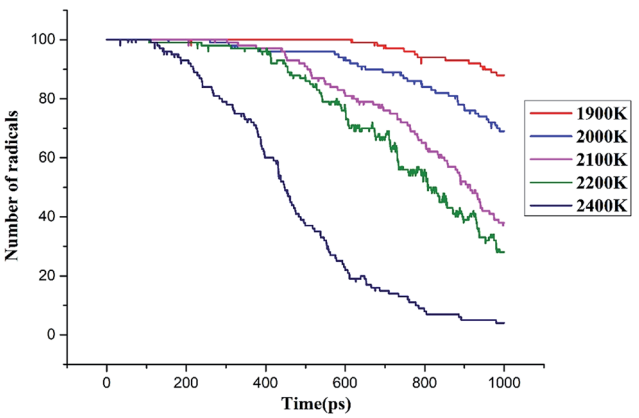

Fig. 5 Time evolution of the C_3F_7CN molecules decomposition when temperature is increased from 1900 to 2400 K (C_3F_7CN system).

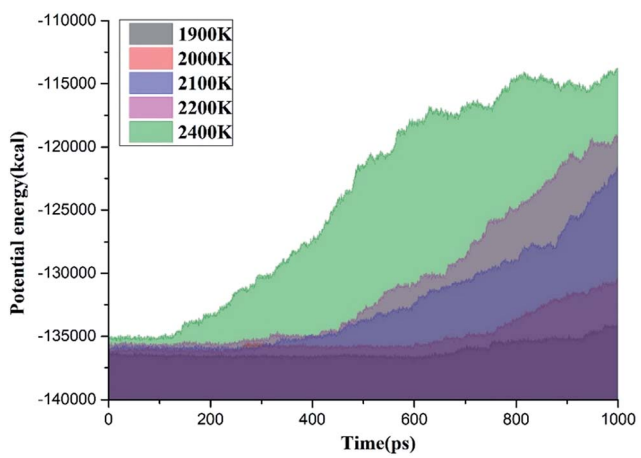

Fig. 4 Time evolution of the potential energy between 1900 K and 2400 K (C_3F_7CN system).

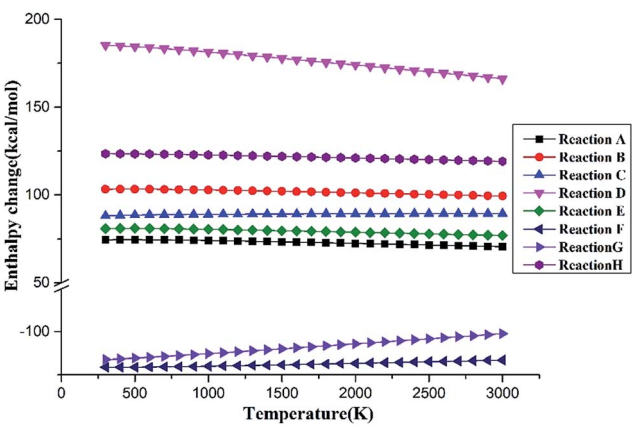

Fig. 6 Enthalpy change of the reaction pathways from 300 K to 3000 K.

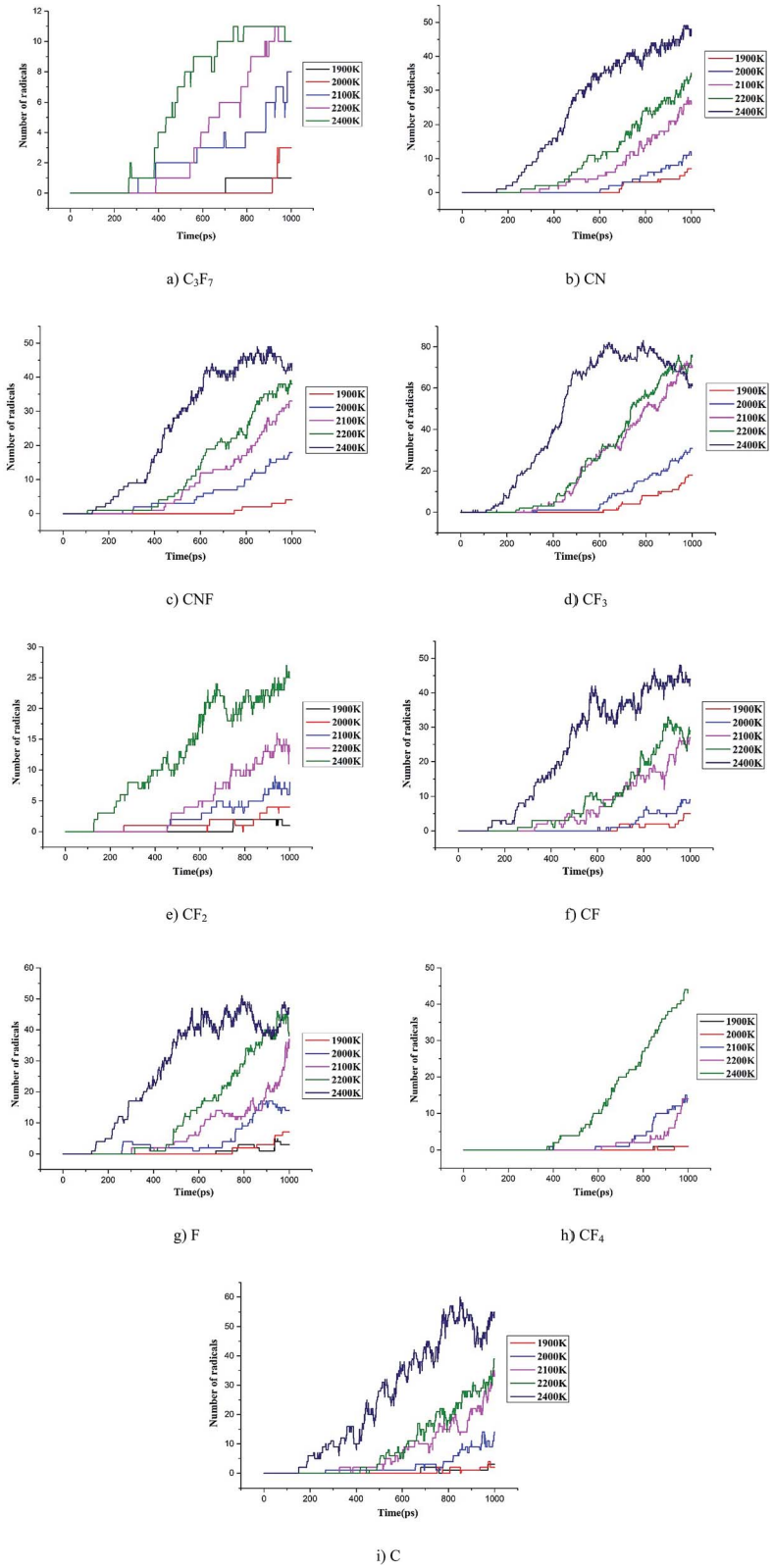

Fig. 7 Time evolution of the major species between 1900 K and 2400 K (C_3F_7CN system).

thereby indicating that the entire decomposition process of C_3F_7CN needs to absorb energy. The growth rate of the potential energy is evidently accelerated with the increase of temperature, indicating that the increase of the ambient temperature will lead to the accelerated decomposition of C_3F_7CN. When the ambient temperature reaches 2400 K, the growth rate of the

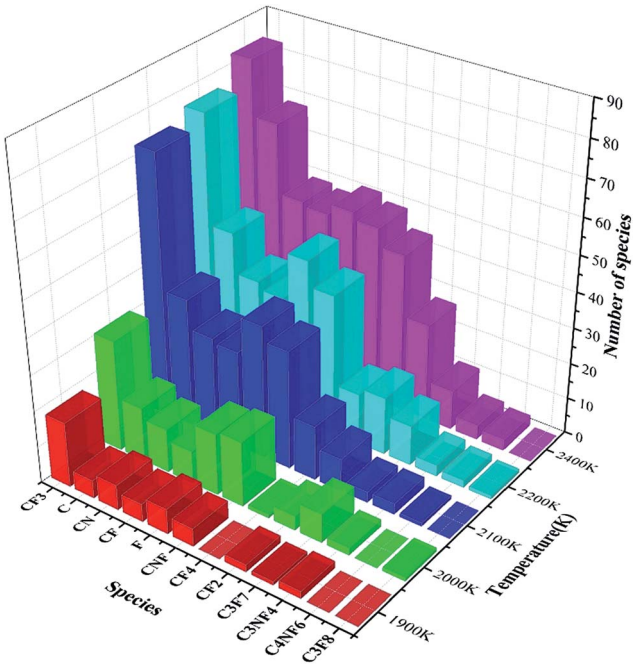

Fig. 8 Number of produced species in C_3F_7CN at different temperatures.

potential energy in the time range of 125 ps to 600 ps is significantly higher than that of 600–1000 ps. This result indicates that the reactions in the system before 600 ps are mainly absorbed energy. Moreover, exothermic reactions may occur in the system after 600 ps, thereby leading to the considerably gradual growth of the overall potential energy.

Fig. 5 illustrates the time evolution of the C_3F_7CN molecules between 1900 K and 2400 K. The decomposition rate and quantity of the C_3F_7CN molecules are evidently accelerated with the increase of temperature. For example, only 8 C_3F_7CN molecules decomposed at 1900 K, whereas 96 C_3F_7CN molecules decomposed at 2400 K at the end of the molecular dynamic simulation.

To further analyze the effect of temperature on the decomposition of C_3F_7CN, the enthalpy of the main reaction paths in the temperature range of 300–3000 K is calculated based on DFT (see Fig. 6). As the temperature increases, the reaction enthalpy of paths A, B, D, and E decreases, that is, the temperature increase is favorable for the reaction progress. The enthalpy change of path D is the most evident, thereby indicating that the increase of temperature has a significant effect on the decomposition of CF_3CFCN. The reaction enthalpy change of paths C and H is not significantly with increasing temperature. Paths F and G are exothermic reaction processes and the energy released decreases as the temperature increases.

3.1.3 Intermediates and main products. Fig. 7 illustrates the time evolution of the major species of C_3F_7CN decomposition over the temperature range from 1900 K to 2400 K. Fig. 8 shows the maximum number of produced species. The statistical results in Fig. 7 shows that the amount of C_3F_7, CN, CNF, CF_3, CF_2, CF, $CF_3CFCN(C_3NF_4)$, F, and other free radicals and CF_4 produced by the decomposition of C_3F_7CN increased with the increase of temperature.

The statistical results in Fig. 8 show that the content of CF_3 at each temperature is the highest among all the products, while the contents of CF_2, CN, CNF, and F are similar. The contents of C_3F_7, C_3NF_4, and C_4NF_6 are lower compared with those of other products. C_4NF_6 is generated by the dissociation of the F atom in the C_3F_7CN molecule from the central C atom (C2 atom as shown in Fig. 1), thereby requiring the absorption of 89.17 kcal mol^{-1}. In addition, a few small stable molecules, such as CF_4 and C_3F_8, are found during the simulation. The generation rate of CF_4 in the time range of 600–1000 ps at 2400 K increased and the amount of CF_3 and F during the time range reduced (as shown in Fig. 7). Given that the generation path of CF_4 (path G in Table 1) is exothermic, the gradual growth of the overall potential energy of the system is actually due to the large amount of CF_4 produced.

3.2 Decomposition of the C_3F_7CN/CO_2 mixture

3.2.1 Effect of temperature on the decomposition process. In order to obtain the decomposition properties of the insulating medium in a practical application condition, the

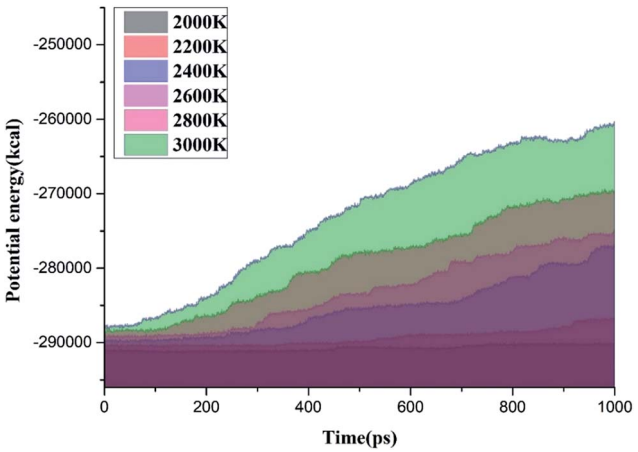

Fig. 9 Time evolution of the potential energy between 2000 K and 3000 K (C_3F_7CN/CO_2 system).

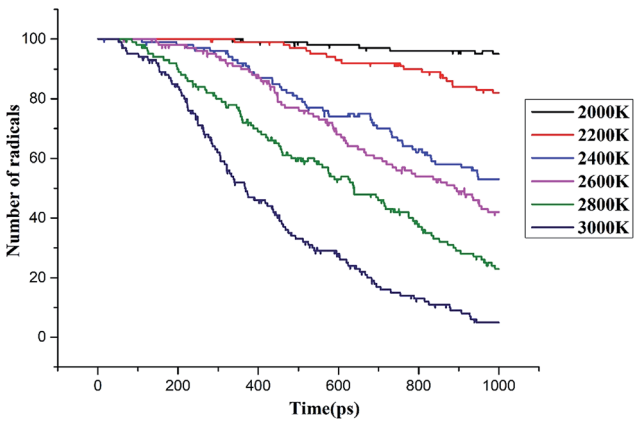

Fig. 10 Time evolution of the C_3F_7CN molecules decomposition when temperature is increased from 2000 to 3000 K (C_3F_7CN/CO_2 system).

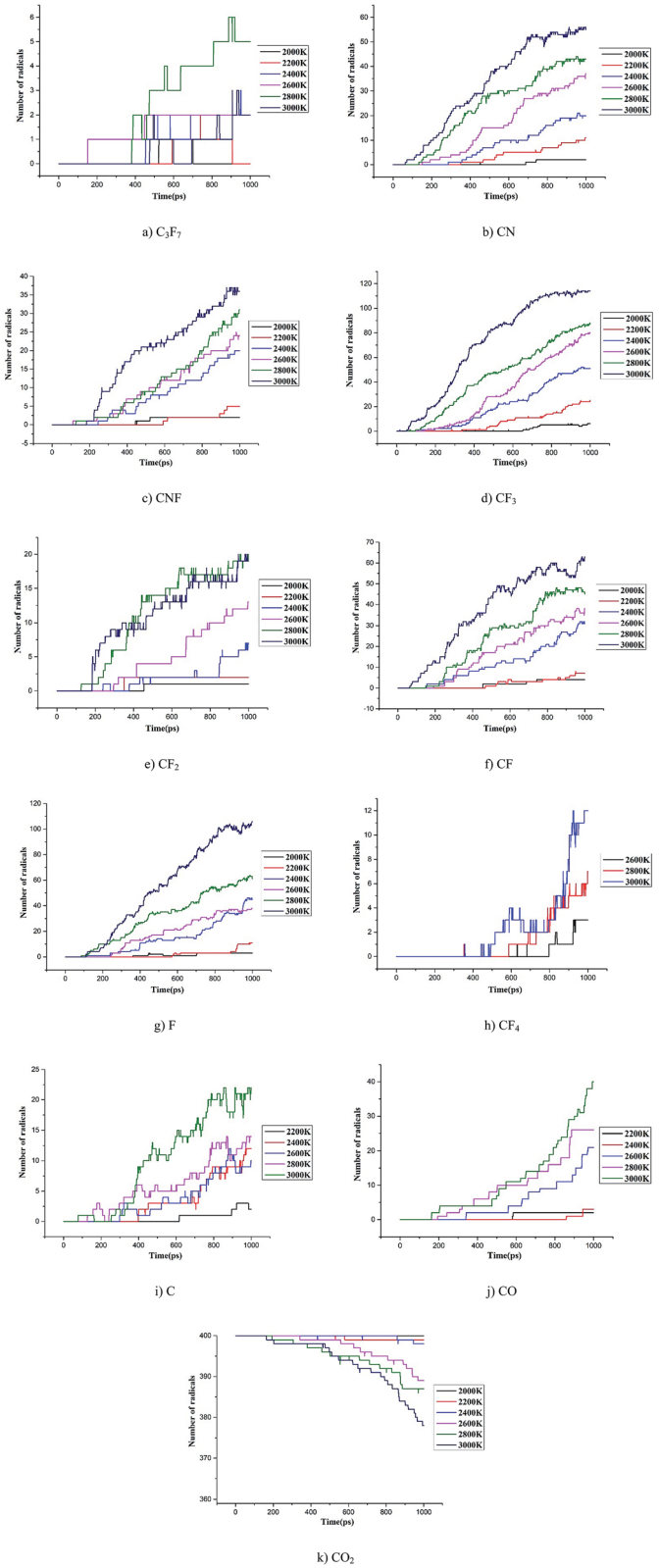

Fig. 11 Time evolution of the major species between 2000 K and 3000 K (C_3F_7CN/CO_2 system).

decomposition characteristics of C_3F_7CN/CO_2 gas mixture over the temperature range from 2000 K to 3000 K were discussed. Fig. 9 shows the time evolution of the potential energy of the

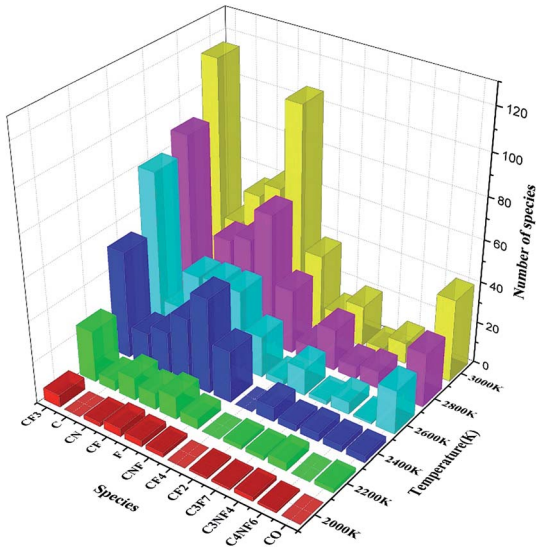

Fig. 12 Number of produced species in C_3F_7CN/CO_2 at different temperatures.

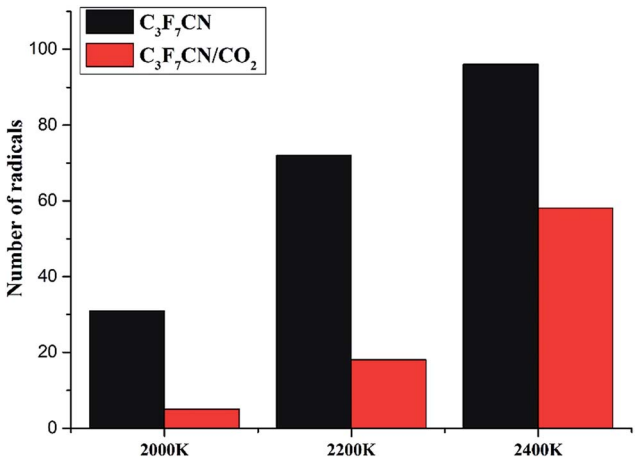

Fig. 13 Final decomposition amount of C_3F_7CN at different temperatures.

C_3F_7CN/CO_2 gas mixture system. Fig. 10 provides the decomposition amount of C_3F_7CN.

The potential energy of the system shows an increasing trend in the range of 2200–3000 K. When the ambient temperature is above 2400 K, the potential energy of the system increases. When the ambient temperature is 2000 K, the potential energy of the system does not change substantially, thereby exhibiting a relationship with the decomposition degree when C_3F_7CN is low. The decomposition rate of C_3F_7CN is accelerated with the increase of temperature, thereby showing consistency with the conclusion of the pure C_3F_7CN system.

3.2.2 Intermediates and main products. Fig. 11 describes the time evolution of the major decomposition species of C_3F_7CN over the temperature range from 2000 K to 3000 K. Fig. 12 presents the maximum number of produced species.

Table 2 Final amount of the decomposition products at different temperatures

	Temperature					
	2000 K		2200 K		2400 K	
Major species	C_3F_7CN	C_3F_7CN/CO_2	C_3F_7CN	C_3F_7CN/CO_2	C_3F_7CN	C_3F_7CN/CO_2
C_3F_7	8	1	11	2	11	3
CF_3	31	6	76	25	83	52
CF_2	4	1	16	2	27	7
CF	9	4	33	8	48	32
CN	12	2	35	11	49	21
CNF	18	2	39	5	49	25
F	17	3	46	11	51	46
C_3NF_4	2	2	3	4	4	4
C_4NF_6	0	1	2	0	3	3
CF_4	1	0	14	0	44	0
C	15	0	46	5	68	16

Similar to the pure C_3F_7CN system, the content of the major decomposition products shows an increasing trend with the increase of temperature. The content of CF_3 in the products is the highest at each temperature. When the temperature is below 2800 K, the yields of CN, CNF, CF, and F are similar. When the temperature is above 2800 K, the content of F in the system increases. A new decomposition of products, namely, CO, is produced due to the addition of CO_2. The decomposition of CO_2 accelerated at temperatures over 2600 K and 40 molecules of CO are produced at 3000 K. In the C_3F_7CN/CO_2 system, the yield of CF_4 reduces. Only 12 CF_4 molecules were produced at 3000 K at the end of the simulation, which is lower than that of the pure C_3F_7CN system. In addition, the generation rate of CF_3 and F after 800 ps at 3000 K slowed down, which is related to the formation of CF_4.

3.2.3 Effect of CO_2 on the decomposition process. Fig. 13 shows the final decomposition amount of C_3F_7CN in C_3F_7CN and C_3F_7CN/CO_2 system at the same temperature. The decomposition amount of C_3F_7CN in the C_3F_7CN/CO_2 gas mixture system is lower than that in the pure C_3F_7CN system at the same temperature. For example, the decomposition amount in the pure C_3F_7CN system is 96 at 2400 K, whereas that of the C_3F_7CN/CO_2 gas mixture system is 58. The addition of the buffer gas CO_2 can effectively inhibit the decomposition of C_3F_7CN.

Table 2 shows that the final amount of the decomposition products in the C_3F_7CN/CO_2 gas mixture system is lower than that in the pure C_3F_7CN system at the same temperature. Moreover, the addition of CO_2 inhibits the formation of CF_4 and C, thereby making it difficult for the system to precipitate carbon and produce products with relatively poor insulation properties. This result is beneficial to protect the insulation properties of the system.

Therefore, the C_3F_7CN/CO_2 gas mixture is relatively suitable for using as a gas-insulated medium relative to pure C_3F_7CN. The mechanism of the action of CO_2 over C_3F_7CN to avoid its decomposition process in function of temperature needs further study.

4 Conclusion

This study analyzed the decomposition characteristics of C_3F_7CN and its gas mixture based on ReaxFF-MD method and density functional theory. The main decomposition pathways, reaction enthalpy, and the composition of the main decomposition products of C_3F_7CN at different temperatures were revealed. The decomposition characteristics of C_3F_7CN and C_3F_7CN/CO_2 gas mixture were compared and analyzed.

The decomposition of C_3F_7CN mainly produces CF_3, C_3F_7, CN, CNF, CF_2, CF, F, and other free radicals and a few molecular products, such as CF_4 and C_3F_8. The decomposition rate of C_3F_7CN and generation rate of the products increase with the increase of ambient temperature. The C_3F_7CN/CO_2 gas mixture has more excellent decomposition characteristics than that of pure C_3F_7CN at the same condition, which is relatively suitable for use as a gas-insulated medium in electrical equipment.

Conflicts of interest

There are no conflicts to declare.

Acknowledgements

The current work is supported by the science and technology project of China Southern Power Grid (No. CSGTRC-K163010)

References

1 A. Beroual and A. Haddad, Recent Advances in the Quest for a New Insulation Gas with a Low Impact on the Environment to Replace Sulfur Hexafluoride (SF_6) Gas in High-Voltage Power Network Applications, *Energies*, 2017, **10**(8), 1216.
2 X. Zhang, Y. Li, S. Xiao, *et al.*, Decomposition mechanism of $C_5F_{10}O$: An environmentally friendly insulation medium, *Environ. Sci. Technol.*, 2017, **51**(17), 10127–10136.
3 J. Reilly, R. Prinn, J. Harnisch, *et al.*, Multi-gas assessment of the Kyoto Protocol, *Nature*, 1999, **401**(6753), 549.

4 Y. Kieffel, T. Irwin, P. Ponchon, *et al.*, Green Gas to Replace SF_6 in Electrical Grids, *IEEE Power and Energy Magazine*, 2016, **14**(2), 32–39.
5 M. P. Sulbaek Andersen, M. Kyte, S. T. Andersen, *et al.*, Atmospheric Chemistry of $(CF_3)_2CFCN$: A Replacement Compound for the Most Potent Industrial Greenhouse Gas, SF_6, *Environ. Sci. Technol.*, 2017, **51**(3), 1321–1329.
6 Z. Lv, D. Zhao and S. Xu, Facile synthesis of mesoporous melamine-formaldehyde spheres for carbon dioxide capture, *RSC Adv.*, 2016, **6**(64), 59619–59623.
7 J. G. Owens, Greenhouse gas emission reductions through use of a sustainable alternative to SF_6, *IEEE Electrical Insulation Conference (EIC)*, Montréal, Canada, 2016, pp. 535–538.
8 Y. Kieffel, Characteristics of g3-an alternative to SF_6, *IEEE International Conference on Dielectrics(ICD)*, Montpellier, France, 2016, vol. 2, pp. 880–884.
9 H. E. Nechmi, A. Beroual, A. Girodet, *et al.*, Fluoronitriles/CO_2 Gas Mixture as Promising Substitute to SF6 for Insulation in High Voltage Applications, *IEEE Trans. Dielectr. Electr. Insul.*, 2016, **23**(5), 2587–2593.
10 C. Preve, R. Maladen and D. Piccoz, Method for validation of new eco-friendly insulating gases for medium voltage equipment, *IEEE International Conference on Dielectrics (ICD)*, Montpellier, France, 2016, vol. 1, pp. 235–240.
11 M. P. S. Andersen, M. Kyte, S. T. Andersen, C. J. Nielsen and O. J. Nielsen, Atmospheric Chemistry of $(CF_3)_2CF–CN$: A Replacement Compound for the Most Potent Industrial Greenhouse Gas, SF_6, *Environ. Sci. Technol.*, 2017, **51**(3), 1321–1329.
12 X. Zhang, Y. Li, S. Xiao, *et al.*, Theoretical study of the decomposition mechanism of environmentally friendly insulating medium C_3F_7CN in the presence of H_2O in a discharge, *J. Phys. D: Appl. Phys.*, 2017, **50**(32), 325201.
13 A. C. T. V. Duin, S. Dasgupta, F. Lorant, *et al.*, ReaxFF: A Reactive Force Field for Hydrocarbons, *J. Phys. Chem. A*, 2001, **105**(41), 9396–9409.
14 J. Zhang, Y. Si, C. Leng, *et al.*, Molecular dynamics simulation of Al–SiO_2 sandwich nanostructure melting and low-temperature energetic reaction behavior, *RSC Adv.*, 2016, **6**(64), 59313–59318.
15 S. Bhoi, T. Banerjee and K. Mohanty, Insights on the combustion and pyrolysis behavior of three different ranks of coals using reactive molecular dynamics simulation, *RSC Adv.*, 2016, **6**(4), 2559–2570.
16 D. Hong, L. Liu, Y. Huang, *et al.*, Chemical effect of H_2O on CH_4 oxidation during combustion in O_2/H_2O environments, *Energy Fuels*, 2016, **30**(10), 8491–8498.
17 H. J. C. Berendsen, J. P. M. Postma, W. F. V. Gunsteren, *et al.*, Molecular dynamics with coupling to an external bath, *J. Chem. Phys.*, 1984, **81**(8), 3684–3690.
18 G. Te Velde, F. M. Bickelhaupt, E. J. Baerends, *et al.*, Chemistry with ADF, *J. Comput. Chem.*, 2001, **22**(9), 931–967.
19 T. C. Ngo, D. Q. Dao, M. T. Nguyen, *et al.*, A DFT analysis on the radical scavenging activity of oxygenated terpenoids present in the extract of the buds of Cleistocalyx operculatus, *RSC Adv.*, 2017, **7**(63), 39686–39698.
20 Q. Zhou, X. Su, W. Ju, *et al.*, Adsorption of H2S on graphane decorated with Fe, Co and Cu: a DFT study, *RSC Adv.*, 2017, **7**(50), 31457–31465.
21 P. Zhang, X. Hou, J. Mi, *et al.*, Curvature Effect of SiC Nanotubes and Sheet for CO_2 Capture and Reduction, *RSC Adv.*, 2014, **4**(90), 48994–48999.
22 Y. Zhao and D. G. Truhlar, The M06 suite of density functionals for main group thermochemistry, thermochemical kinetics, noncovalent interactions, excited states, and transition elements: two new functionals and systematic testing of four M06-class functionals and 12 other functionals, *Theoretical Chemistry Accounts: Theory, Computation, and Modeling*, 2008, **120**(1), 215–241.
23 Y. Zhao and D. G. Truhlar, A new local density functional for main-group thermochemistry, transition metal bonding, thermochemical kinetics, and noncovalent interactions, *J. Chem. Phys.*, 2006, **125**(19), 194101.
24 A. S. Menon and L. Radom, Consequences of spin contamination in unrestricted calculations on open-shell species: effect of Hartree-Fock and Møller-Plesset contributions in hybrid and double-hybrid density functional theory approaches, *J. Phys. Chem. A*, 2008, **112**(50), 13225–13230.
25 X. Zhang, S. Xiao, J. Zhang, *et al.*, Influence of humidity on the decomposition products and insulating characteristics of CF_3I, *IEEE Trans. Dielectr. Electr. Insul.*, 2016, **23**(2), 819–828.
26 R. Ono and T. Oda, Measurement of gas temperature and OH density in the afterglow of pulsed positive corona discharge, *J. Phys. D: Appl. Phys.*, 2008, **41**(3), 035204.
27 Y. Fu, M. Rong, K. Yang, *et al.*, Calculated rate constants of the chemical reactions involving the main byproducts SO_2F, SOF_2, SO_2F_2 of SF_6 decomposition in power equipment, *J. Phys. D: Appl. Phys.*, 2016, **49**(15), 155502.
28 H. Tanaka, D. Tanahashi, Y. Baba, *et al.*, Finite-difference time-domain simulation of partial discharges in a gas insulated switchgear, *High Voltage*, 2016, **1**(1), 52–56.
29 Z. Chen, W. Sun and L. Zhao, High-temperature and High-pressure Pyrolysis of Hexadecane: A Molecular Dynamic Simulation Based on Reactive Force Field (ReaxFF), *J. Phys. Chem. A*, 2017, **121**(10), 2069.